Supporting information

Dry reforming of methane in an atmospheric pressure glow discharge: confining the plasma to expand the performance

Bart Wanten, Stein Maerivoet, Christine Vantomme, Joachim Slaets, Georgi Trenchev, Annemie Bogaerts

Research group PLASMANT, University of Antwerp, Department of Chemistry, Universiteitsplein 1, B-2610 Antwerp, Belgium

1 Details on experimental analysis

1.1 Gas and liquid analysis

The equipment used for gas analysis is a Thermo Scientific Trace 1310 gas chromatograph (TGC). The TGC contains two separate ovens, one containing the different columns while the other contains all valves and sample loops. The incoming gas flow is sampled at constant pressure in a set of 100 µL sample loops positioned in a valve oven. With helium used as carrier gas, the sample is sent onto two consecutive Rt-Q-BOND columns, which separates the permanent gasses H_2, O_2, N_2, CO and CH_4 from CO_2 and lower hydrocarbons (up to C_3), while more polar molecules like H_2O are backflushed. Afterwards the sample passes one molsieve 5A column, which will separate the permanent gasses from each other, while CO_2 and hydrocarbons by-pass this column. The sample arrives on a thermal conductivity detector (TCD). Calibration was performed for the gasses CO_2, CH_4, N_2, O_2, CO, H_2, C_2H_2, C_2H_4 and C_2H_6.

A liquid sample collected at 25% CH_4, 20 mA and 1 L/min was also analysed. A Thermo Focus SSL GC with Stabilwax column and FID was used to quantify methanol in the sample. The same sample was also analysed by means of a Waters alliance 2695 HPLC, containing a Shodex RSpak KC-811 column, PDA (photo-diode array) 2996 detector and RI (refractive index) 2414 detector. Formaldehyde and acetic acid could be detected. For both GC and HPLC analysis, 100 ppm standard solutions in water and an internal standard was used for proper identification and quantification.

1.2 Correction factors α, β and α'

Because of the gas expansion inherent to DRM, the flow rate changes between the reactor in- and outlet. When the same volume is sampled at constant pressure, the concentration of the unconverted reactants would be underestimated. Furthermore, since some products condense and are not present anymore in the GC's sample mixture, it would also lead to a change in concentration of the remaining components. If not taken into account, these effects can lead to significant errors regarding conversion, selectivity, etc. Figure S.1 shows a schematic representation of the different effects during our measurements that lead to changes in concentration of the components in the output gas mixture.

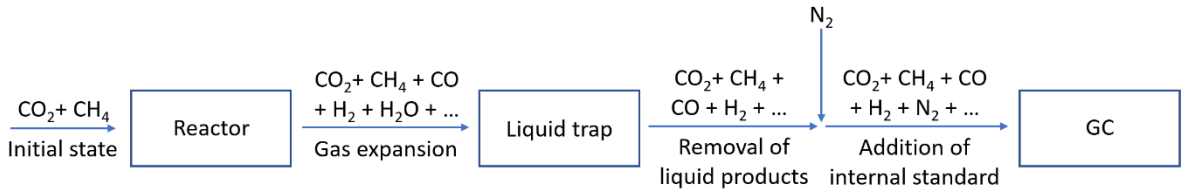

Figure S.1: Schematic overview of different steps between the reactor inlet and GC that influence the measured concentrations.

To correct for these effects, N_2 is used as an internal standard and added to the gas mixture after the reactor outlet. In this way, two correction factors can be defined:

$$\alpha = \frac{\varphi_{plasma}}{\varphi_{blanc}} = \frac{A_{IS}^{blanc}}{A_{IS}^{plasma}}(1+\beta) - \beta \qquad (S.E1)$$

$$\beta = \frac{\varphi_{IS}}{\varphi_{blanc}} = 0.1 \qquad (S.E2)$$

The factor β is defined as the flow rate of the internal standard with respect to the flow rate at the reactor inlet, and was always kept at 10%. The factor α corrects for the overall change in flow rate when comparing a blank to a plasma measurement, and can be expressed as a function of β and the peak areas of the internal standard for a blank and plasma measurement. These factors are derived from the work of Pinhão et al.[1]

Note that α corrects for both gas expansion and the removal of liquid products. To obtain the factor that is a measure for gas expansion only, the sum of the concentrations of all components that make up the liquid fraction, $\sum_k c_k'$, has to be known:

$$\alpha' = \frac{\alpha}{(1 - \sum_k c_k')} \qquad (S.E3)$$

This will be further discussed in section 1.4.

1.3 Experimental formulas

1.3.1 Concentrations

The concentrations for each reactant i and product j, corrected for the dilution by the addition of an internal standard, can be defined for a blank and plasma measurement as:

$$c_i^{blanc} = c_{i,m}^{blanc}\left(1 + \frac{\varphi_{IS}}{\varphi_{blanc}}\right) = c_{i,m}^{blanc}(1+\beta) \qquad (S.E4)$$

$$c_i^{plasma} = c_{i,m}^{plasma}\left(1 + \frac{\varphi_{IS}}{\varphi_{plasma}}\right) = c_{i,m}^{plasma}\left(1 + \frac{\beta}{\alpha}\right) \qquad (S.E5)$$

$$c_j^{plasma} = c_{j,m}^{plasma}\left(1 + \frac{\varphi_{IS}}{\varphi_{plasma}}\right) = c_{j,m}^{plasma}\left(1 + \frac{\beta}{\alpha}\right) \qquad (S.E6)$$

With c_m being for the concentration measured at the GC.

1.3.2 Conversion

The conversion of a single reactant is expressed in terms of the concentrations, defined in equation (S.E4) and (S.E5), and the correction factor α, defined in equation (S.E1):

$$X_i = \frac{c_i^{blanc} - \alpha \cdot c_i^{plasma}}{c_i^{blanc}} = 1 - \frac{\alpha \cdot c_i^{plasma}}{c_i^{blanc}} \quad (S.E7)$$

The total conversion is defined as the weighted average of the conversion for each reactant, weighted over their concentration in the inlet gas mixture:

$$X^{tot} = \sum_i c_i^{blanc} \cdot X_i \quad (S.E8)$$

1.3.3 Energy cost

The total energy cost (EC, kJ/L) is expressed in terms of the total conversion and the specific energy input (SEI, kJ/L):

$$EC\left(\frac{kJ}{L}\right) = \frac{SEI\left(\frac{kJ}{L}\right)}{X^{tot}} \quad (S.E9)$$

With SEI defined as the plasma power P_{plasma} (kW) over the total inlet flow rate φ_{blanc} (L/s, normal conditions):

$$SEI\left(\frac{kJ}{L}\right) = \frac{P_{plasma}(kW)}{\varphi_{blanc}\left(\frac{L}{s}\right)} \quad (S.E10)$$

Note that equation (S.E9) can also be expressed in terms of eV/molecule:

$$EC\left(\frac{eV}{molecule}\right) = \frac{SEI\left(\frac{kJ}{L}\right)}{X^{tot}} \cdot \frac{V_{mol}\left(\frac{L}{mol}\right) \cdot \frac{6.24 \cdot 10^{21} eV}{kJ}}{\frac{6.02 \cdot 10^{23} molecules}{mol}} \quad (S.E11)$$

With V_{mol} the molar volume, equal to 24.05 L/mol (normal conditions).

1.3.4 Selectivity and yield

The selectivity is defined as the amount of atoms a that end up in product j, with respect to the amount of atoms a that are available through conversion of the reactant(s) i. In equation form, this becomes:

$$S_{j,a} = \frac{\mu_{j,a} \cdot \alpha \cdot c_j^{out}}{\sum_i \mu_{i,a} \cdot \left(c_i^{in} - \alpha \cdot c_i^{out}\right)} \quad (S.E12)$$

The yield is defined as the actual amount of product j formed with respect to the maximum amount that could be formed theoretically, based on atom a. In equation form this becomes:

$$Y_{j,a} = \frac{\mu_{j,a} \cdot \alpha \cdot c_j^{out}}{\sum_i \mu_{i,a} \cdot c_i^{in}} \quad (S.E13)$$

As a side-note, yield is related to both conversion and selectivity, since it can also be written as:

$$Y_{j,a} = S_{j,a} \cdot \left(\frac{1}{\sum_i \mu_{i,a} \cdot c_i^{in}} \cdot \sum_i \left(\mu_{i,a} \cdot c_i^{in} \cdot X_i\right)\right) = S_{j,a} \cdot X_a \quad (S.E14)$$

With X_a the weighted average of the conversion of any reactant i containing atom a, weighted over the concentration of i in the inlet gas mixture and the amount of atoms a in reactant i. In the case of only CO_2 and CH_4 as inlet gas mixture, X_a is equal to the CO_2 conversion for $a = O$, the CH_4 conversion for $a = H$, and the total conversion for $a = C$.

1.4 Estimating the concentration of H_2O

GC- and HPLC-analysis of the liquid fraction collected at 25% CH_4, 20 mA and 1 L/min showed that it mostly consists of water, with formaldehyde, acetic acid and methanol present at levels of 20-200 ppm. Because of the very low concentration of these components, the liquid fraction itself can be approximated as being pure H_2O.

To calculate the concentration of H_2O in the plasma mixture, we have to look at the atom balances. For the oxygen balance equation, the formula is written as:

$$b_O = \frac{\alpha \cdot \left(\sum_i \mu_{i,O} \cdot c_i^{plasma} + \sum_j \mu_{j,O} \cdot c_j^{plasma}\right) + \alpha' \cdot \sum_k \mu_{k,O} \cdot {c_k}'}{\sum_i \mu_{i,O} \cdot c_i^{blanc}} = 1 \qquad (S.E15)$$

With the correction factor for gas expansion, α', as defined in equation (S.E3). As mentioned, we can state that:

$$\sum_k \mu_{k,O} \cdot {c_k}' \approx {c_{H_2O}}' \qquad (S.E16)$$

With $\mu_{k,O} = 1$. Note that we use here ${c_{H_2O}}'$ and not c_{H_2O}, to specify that it concerns a concentration which is not measured at the GC, and that it correlates with the situation at the end of the plasma reactor, before condensation happens. Equation (S.E15) can then be re-written as:

$$\frac{{c_{H_2O}}'}{\left(1 - {c_{H_2O}}'\right)} = \frac{1}{\alpha} \cdot \sum_i \mu_{i,O} \cdot c_i^{blanc} - \left(\sum_i \mu_{i,O} \cdot c_i^{plasma} + \sum_j \mu_{j,O} \cdot c_j^{plasma}\right) \qquad (S.E17)$$

Since everything on the right-hand side is known (see equations (S.E1), (S.E4), (S.E5) and (S.E6)), ${c_{H_2O}}'$ can be determined. Afterwards also equation E3 can be solved. With both α' and ${c_{H_2O}}'$, the yield and selectivity as defined in equations (S.E12), (S.E13) and (S.E14) can be calculated for H_2O. However, because of its derivation through the atom balance, the error margin on each measured concentration is propagated onto ${c_{H_2O}}'$. This leads to a significantly larger error margin on this value in comparison with the measured concentrations, and the same applies for its selectivity and yield.

2 Details on quasi-1D model

2.1 Set of equations used in the model and important plasma parameters

The continuity or mass conservation equation is solved for every species in ZDPlasKin[2] (see section 2.2) and is based on production and loss rates:

$$\frac{dn_s}{dt} = \sum_r \left[(a_{sr}^R - a_{sr}^L) k_r \prod_l n_l^L \right] \qquad (S.E18)$$

In equation (S.E18), n_s stands for the density of species s (in m^{-3}), a_{sr}^R and a_{sr}^L are the stoichiometric coefficients of species s at the left and right side of reaction r, respectively. n_l is the density of species l on the left side of the reaction and k_r is the reaction rate coefficient of reaction r. Reaction r can be represented in general as follows:

$$a_A A + a_B B\ (+\delta H) \xrightarrow{k_r} a_C C + a_D D\ (+\delta H) \qquad (S.R1)$$

With A, B, C and D the different species and a_A, a_B, a_C and a_D their stoichiometric coefficients. δH represents the reaction enthalpy (in J). The reaction rate coefficients k_r for heavy-particle reactions are derived from literature[3], either as constant or as function of the gas temperature. In case of electron impact reactions, the rate coefficients depend on the electron energy, or more specifically, the electron energy distribution function (EEDF), which depends on the reduced electric field. Through the BOLSIG+ solver[4], built into the ZDPlasKin code, the Boltzmann equation is solved for electrons, resulting in the EEDF. Cross-sections for the different elastic and inelastic collisions are derived from literature[5] and are used to calculate the rate coefficients:

$$k_r = \int_{\varepsilon_{threshold}}^{+\infty} \sigma_r(\varepsilon) f_e(\varepsilon) \sqrt{\frac{2\varepsilon}{m_e}}\, d\varepsilon \qquad (S.E19)$$

In equation (S.E19), ε stands for the electron energy (in eV), $\varepsilon_{threshold}$ is the energy threshold for the reaction (also taken from literature[5]), $\sigma_r(\varepsilon)$ is the cross-section of reaction r (in m^2), $f_e(\varepsilon)$ is the EEDF (in m^{-3} eV^{-1}) and m_e is the mass of an electron, which is equal to 9.1094x10^{-31} kg.

The electric field E (V m^{-1}) is calculated through the local field approximation:

$$E = \sqrt{P/\sigma} \qquad (S.E20)$$

Here P stands for the power density (in W m^{-3}) and σ stands for the plasma conductivity (in A V^{-1} m^{-1}). Note that to get the reduced electric field, every term should be divided by the total density n_t. The power density is calculated by dividing the experimental plasma power by the plasma volume, which itself is estimated, as will be further discussed in section 2.5. At the start of the simulation, the plasma conductivity is defined as:

$$\sigma = \frac{e^2 \cdot n_{e,init}}{m_e \cdot \nu_m} \qquad (S.E21)$$

e is the charge of an electron (1.6022x10^{-19} C), $n_{e,init}$ is the initial electron density (in m^{-3}) and ν_m is the collision frequency (in s^{-1}). The plasma conductivity is updated every time step as:

$$\sigma = \frac{e \cdot v_d \cdot n_e}{(E/n_t) \cdot n_t} = e \cdot n_e \cdot \mu_e \qquad (S.E22)$$

v_d is the drift velocity of the electrons (m s^{-1}), calculated with BOLSIG+, (E/n_t) is the reduced electric field (Td) and μ_e is the electron mobility.

In Figure S.2 we present a flow chart, showing the numerical solution of the quasi-1D model by means of the formulas presented in this section. Both the specific role of ZDPlasKin and BOLSIG+ is presented. The flow chart was derived and adapted from S. Kelly et al.[6], who used a very similar approach to obtain a quasi-1D chemical kinetic model.

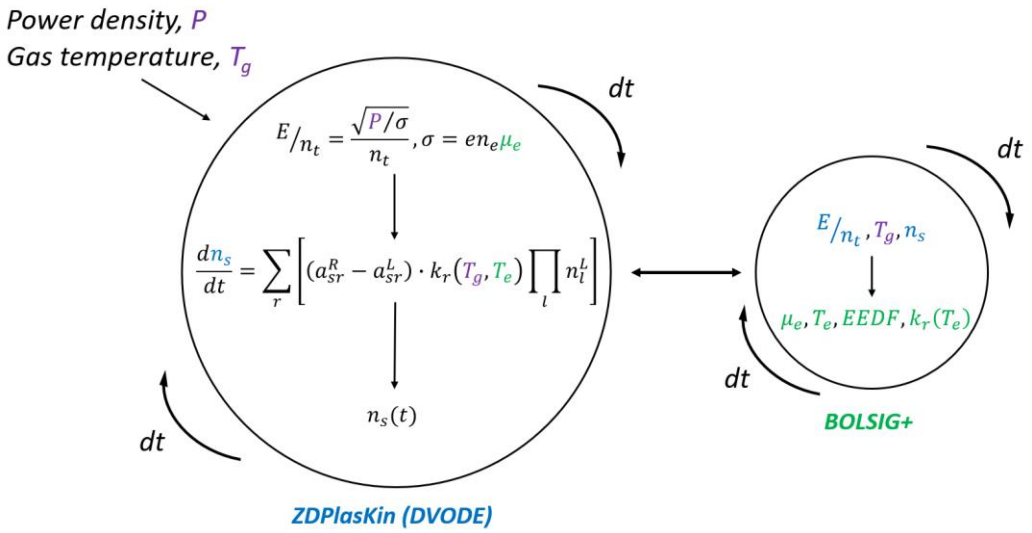

Figure S.2: Flow chart, derived and adapted from S. Kelly et al.[6], of the numerical solution for the quasi-1D model, showing the calculation of the mass balance equation by ZDPlasKin (specifically the DVODE solver; see section 2.2) and the Boltzmann equation by BOLSIG+ each time step. The power density and gas temperature is estimated (see section 2.5) and used as input in the model.

Finally, we present the calculated electron density, electron temperature and reduced electric field (which is the ratio of electric field over gas number density, i.e., an important parameter to characterize gas discharge plasmas) as a function of time for the simulation carried out at 25% CH_4, 30 mA and 1 L/min, in Figure S.3, S.4 and S.5. These results are representative for other conditions as well. The initial electron density is set at $1x10^{10}$ cm^{-3}, and is used to initially solve equation (S.E21). The initial reduced electric field is equal to 50 Td (where 1 Td = 10^{21} V m^3). As can be seen, in the flow chart in Figure S.2, all three parameters are consequently solved each time step through ZDPlasKin and BOLSIG+.

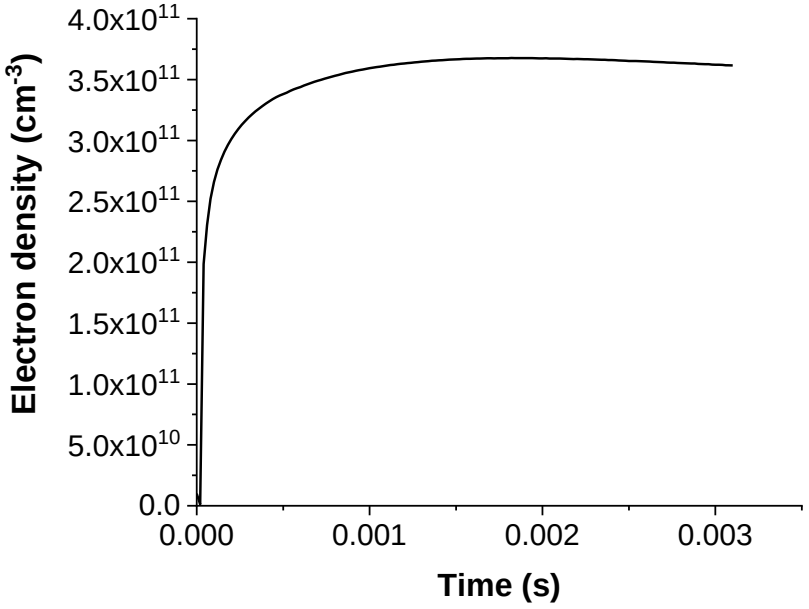

Figure S.3: Calculated electron density as a function of time, at 25% CH_4, 30 mA and 1 L/min. The initial electron density is set at $1x10^{10}$ cm^{-3}.

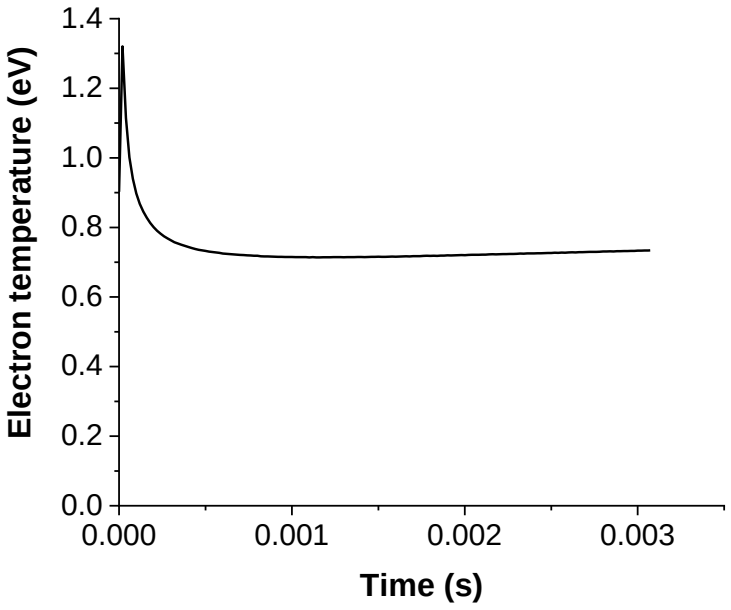

Figure S.4: Calculated electron temperature as a function of time at 25% CH_4, 30 mA and 1 L/min.

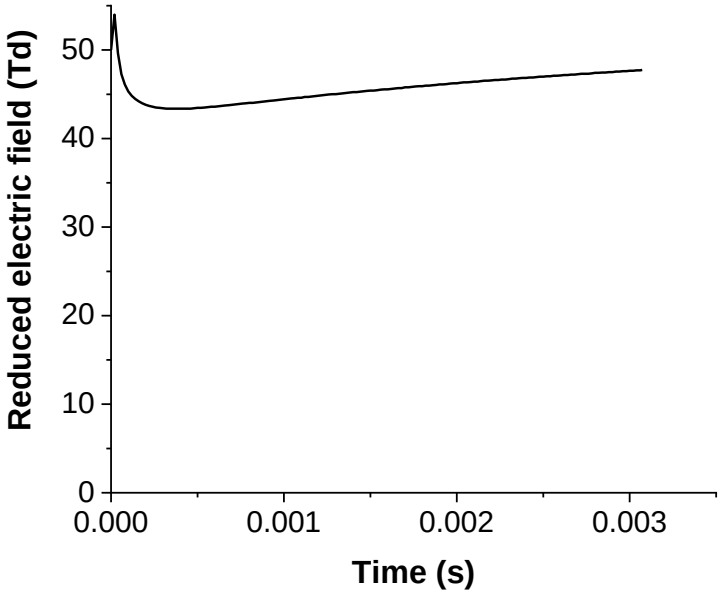

Figure S.5: Reduced electric field as a function of time, at 25% CH_4, 30 mA and 1 L/min. The initial reduced electric field is set at 50 Td.

Since the electron density is initially low, all applied electrical energy is distributed over a limited number of electrons, explaining the early peak in electron temperature. However, this is rather to initially solve the model, but it does not affect the rest of the simulation and the overall calculation results.[8] Eventually, the electron density rises to a value around 3.5×10^{11} cm^{-3}, and remains almost constant. The reduced electric field and electron temperature also reach more or less constant values, around 45 Td and 0.8 eV, respectively. Hence, the plasma is clearly in thermal non-equilibrium (electron temperature is several times higher than the gas temperature). Also, the values of the reduced electric field is relatively low, explaining why vibrational excitation is one of the main mechanisms in the APGD.

2.2 ZDPlasKin

A Fortran 90 module called ZDPlasKin (Zero-Dimensional Plasma Kinetics) is used for the 0D model.[2] A schematic overview of the operation of the module is presented in Figure S.6:

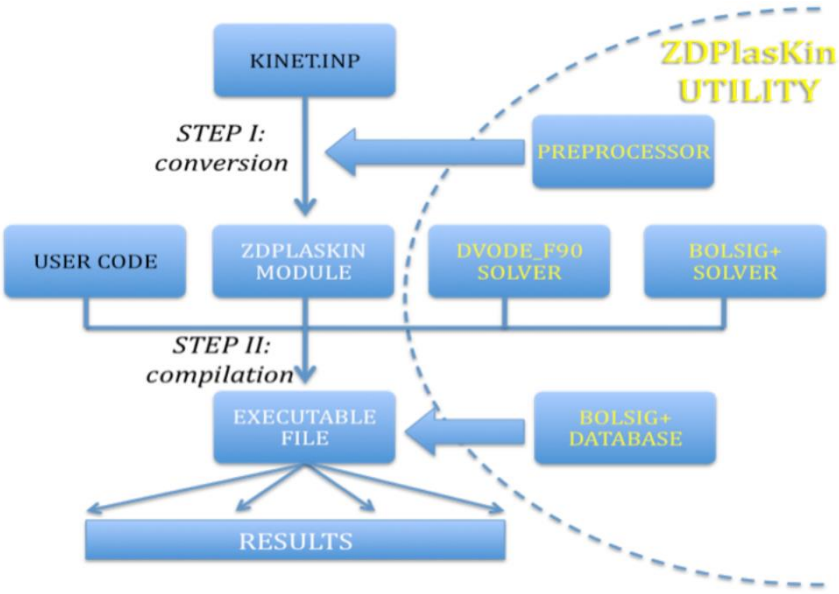

Figure S.6: Schematic overview of the different steps and processes to generate results out of the input used in the 0D model.

As a first step, a pre-processor built into ZDPlasKin converts the data input file kinet.inp (with all species, reactions, rate constants, etc. included) into a Fortran code. Additionally, the pre-processor controls the charge- and mass balance and the uniqueness of each species, reaction, etc. In the second step, an executable file is compiled through the converted kinet.inp file, the user code and two solvers built into ZDPlasKin:

- the DVODE_F90 solver (DVODE = Double precision Variable coefficient Ordinary Differential Equation), which solves all the ordinary differential equations, i.e. the mass balance equations for every species
- the BOLSIG+ solver, which solves the Boltzmann equation for the electrons, resulting in the electron energy distribution function (EEDF).

Cross-sections as a function of energy for every electron impact reaction, which are, in addition to the EEDF, necessary to calculate these rate constants (see equation (S.E21)), are listed in the BOLSIG+ database. Finally, through the executable file, the simulations start and results are generated.

2.3 Chemistry set

In the chemistry set, 123 species are taken into account, consisting of 60 excited species, 24 ions, 20 radicals, and 18 neutral molecules, next to the electrons. These are all listed in Table S.1.

Table S.1: Overview of all species included in the chemistry set of the quasi-1D model.

Neutral molecules	Charged species	Radicals	Excited molecules
	H^+, H_3^+, e^-	H	
CO_2	CO_2^+		$CO_2(V_{A-D})$, $CO_2(V_{1-21})$, $CO_2(E_1)$
CO	CO^+, CO_3^-, CO_4^-		$CO(V_{1-10})$, $CO(E_{1-4})$
O_2	O^-, O^{2-}	O	$O_2(V_{1-4})$, $O_2(E_{1,2})$
CH_4	CH_5^+, CH_4^+,CH_3^+, CH_2^+, CH^+	CH_3, CH_2, CH	
H_2	H_2^+		$H_2(V_{1-14})$
C_3H_8, C_3H_6, C_2H_6, C_2H_4, C_2H_2	$C_2H_6^+$, $C_2H_5^+$, $C_2H_4^+$, $C_2H_3^+$, $C_2H_2^+$, C_2H^+	C_3H_7, C_3H_5, C_2H_5, C_2H_3, C_2H, C	

H_2O, H_2O_2	H_2O^+, H_3O^+, OH^-, OH^+	HO_2, OH
CH_2O, CH_2CO, CH_3OH, CH_3CHO, CH_3OOH		CHO, CH_2OH, CH_2CHO, CH_3O, CH_3CO, C_2HO, CH_3O_2

Some of the vibrational (V) and/or electronic (E) excited states of CO_2, CO, O_2 and H_2 are included, and presented in Table S.2 together with their energy and (if present) identification. Since the asymmetric stretch mode is the most important towards the dissociation of CO_2 in plasma[7,9], all 21 levels up to the dissociation limit of 5.5 eV[8] are included in the model. The symmetric stretch and bending modes are less important, hence only four (combined) lower lying levels of them are included (A-D). One electronically excited state is included with a threshold energy of 10.5 eV, because other lower lying levels immediately give rise to dissociation.[8] 10 vibrational and 4 electronic excited levels of CO and 4 vibrational and 2 electronic excited levels of O_2 are included. In case of H_2, 14 vibrational excited levels and no electronic levels are included. For CH_4, no vibrational excited levels are included, because it has been shown in literature that they have a much smaller population than the vibrational levels of CO_2, and they typically exhibit a thermal (Boltzmann) distribution at the investigated conditions.[10,11]

Table S.2: Notation, corresponding energy and identification of excited levels of species listed in Table S.1.

	Notation	**Energy (eV)**	**Identification**
Electronically excited levels of CO_2	CO_2 (E_1)	10.5	$^1\Delta_u$
Symmetric vibration modes of CO_2	CO_2 (V_A)	0.083	(0 1 0)
	CO_2 (V_B)	0.167	(0 2 0) + (1 0 0)
	CO_2 (V_C)	0.252	(0 3 0) + (1 1 0)
	CO_2 (V_D)	0.339	(0 4 0) + (1 2 0) + (2 0 0)
Asymmetric vibration modes of CO_2	CO_2 (V_1)	0.29	(0 0 1)
	CO_2 (V_2)	0.58	(0 0 2)
	CO_2 (V_3)	0.86	(0 0 3)
	CO_2 (V_4)	1.14	(0 0 4)
	CO_2 (V_5)	1.43	(0 0 5)
	CO_2 (V_6)	1.70	(0 0 6)
	CO_2 (V_7)	1.97	(0 0 7)
	CO_2 (V_8)	2.24	(0 0 8)
	CO_2 (V_9)	2.51	(0 0 9)
	CO_2 (V_{10})	2.77	(0 0 10)
	CO_2 (V_{11})	3.03	(0 0 11)
	CO_2 (V_{12})	3.29	(0 0 12)
	CO_2 (V_{13})	3.55	(0 0 13)
	CO_2 (V_{14})	3.80	(0 0 14)
	CO_2 (V_{15})	4.04	(0 0 15)
	CO_2 (V_{16})	4.29	(0 0 16)
	CO_2 (V_{17})	4.53	(0 0 17)
	CO_2 (V_{18})	4.77	(0 0 18)
	CO_2 (V_{19})	5.01	(0 0 19)
	CO_2 (V_{20})	5.24	(0 0 20)

	CO_2 (V_{21})	5.47	(0 0 21)
Electronically excited levels of CO	CO (E_1)	6.22	$A^3\Pi$
	CO (E_2)	7.90	$A^1\Pi$
	CO (E_3)	10.4	$A^3\Sigma$, $D^3\Delta$, $E^3\Sigma$, $B^3\Sigma$
	CO (E_4)	10.6	$C^1\Sigma$, $E^1\Pi$, $B^1\Sigma$, $I^1\Sigma$, $D^1\Delta$
Vibrationally excited levels of CO	CO (V_1)	0.266	
	CO (V_2)	0.528	
	CO (V_3)	0.787	
	CO (V_4)	1.040	
	CO (V_5)	1.300	
	CO (V_6)	1.540	
	CO (V_7)	1.790	
	CO (V_8)	2.030	
	CO (V_9)	2.270	
	CO (V_{10})	2.510	
Electronically excited levels of O_2	O_2 (E_1)	0.98	$A^1\Delta$, $B^1\Sigma$
	O_2 (E_2)	8.40	$B^3\Sigma$
Vibrationally excited levels of O_2	O_2 (V_1)	0.19	
	O_2 (V_2)	0.38	
	O_2 (V_3)	0.57	
	O_2 (V_4)	0.75	
Vibrationally excited levels of H_2	H_2 (V_1)	0.516	
	H_2 (V_2)	1.001	
	H_2 (V_3)	1.457	
	H_2 (V_4)	1.882	
	H_2 (V_5)	2.277	
	H_2 (V_6)	2.642	
	H_2 (V_7)	2.977	
	H_2 (V_8)	3.282	
	H_2 (V_9)	3.557	
	H_2 (V_{10})	3.802	
	H_2 (V_{11})	4.017	
	H_2 (V_{12})	4.201	
	H_2 (V_{13})	4.356	
	H_2 (V_{14})	4.480	

2.4 Quasi-1D approach

As is clear from section 2.1, equation S.E18, the species densities are calculated only as a function of time. However, we can assume a constant velocity in the axial direction, so that the change as a function of time is translated into a change of the species densities as a function of axial position as well. This is conceptually presented in Figure S.7.

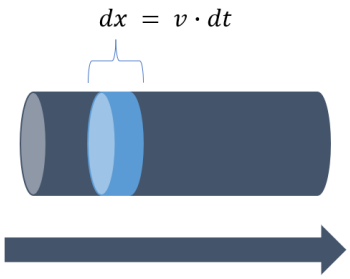

Figure S.7: Schematic representation of the quasi-1D approach towards the species densities.

Therefore, the continuity equation as a function of time (equation (S.E18) above) can also be rewritten as a continuity equation as a function of axial position, in equation (S.E23):

$$\frac{dn_s}{dx} = \frac{1}{v} \cdot \sum_r \left[(a_{sr}^R - a_{sr}^L) k_r \prod_l n_l^L \right] \qquad (S.E23)$$

2.5 Temperature and velocity profile

Fluid simulations for pure CO_2 in an APGD show that the width of the glow discharge is more or less 4 mm, with the largest temperatures and plasma densities located in the centre of the glow discharge[7]. This also means that there is some space of about 0.5 mm wide with no conversion by the plasma. However, we can assume that (i) there will be additional thermal conversion in a zone surrounding the plasma, explaining the high conversion obtained experimentally, and (ii) very close to the wall there will be heat losses, giving rise to a very small zone where additional conversion is negligible. Based on these assumptions, we used a temperature profile as input in our 0D simulations as depicted in Figure S.8.

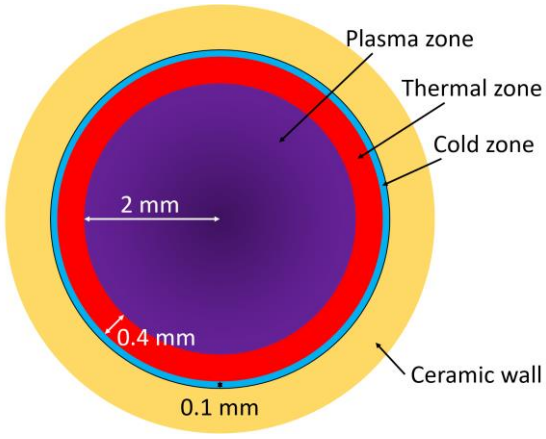

Figure S.8: Schematic representation of the temperature profile assumed for the confined APGD, with each zone and their dimension indicated, surrounded by the ceramic wall.

In this configuration, the plasma and thermal zone fill 92% of the encapsulated zone, which is of the same order as the maximum conversion obtained. The temperature in each zone was assumed to be between 2000 and 3000 K, as was calculated for a pure CO_2 plasma in an APGD[7], and we assumed it to be the same for different CH_4 fractions for the sake of simplicity, while it increases linearly upon rising SEI. Note that the volume of the plasma zone was also used to calculated the power density, as mentioned in section 2.1.

To correct for the fact that the gas does not enter the discharge zone as a laminar flow, but rather as a vortex flow because of the effect of the grooved cathode, a 3D model was designed in COMSOL Multiphysics®. In this model we defined the exact geometry of the confined APGD and we applied a

shear stress transport (SST) turbulent flow model. In this way we could derive the flow velocity for each assumed zone, as these are not uniform, especially for high flow rates.

An overview of the assumed temperatures and calculated axial velocities in each zone, for each combination of current and flow rate, is presented in Table S.3.

Table S.3: Overview of the temperatures and axial velocities for the plasma and thermal zone, used as input in the quasi-1D model.

Condition	Plasma zone		Thermal zone	
	Temperature (K)	Flow velocity (m^3/s)	Temperature (K)	Flow velocity (m^3/s)
25 mA, 2 L/min	2000	1.03×10^{-5}	1600	6.59×10^{-5}
20 mA, 1 L/min	2200	8.07×10^{-6}	1800	2.55×10^{-5}
25 mA, 1 L/min	2300	8.07×10^{-6}	1900	2.55×10^{-5}
30 mA, 1 L/min	2400	8.07×10^{-6}	2000	2.55×10^{-5}
35 mA, 1 L/min	2500	8.07×10^{-6}	2100	2.55×10^{-5}
25 mA, 0.5 L/min	2700	5.43×10^{-6}	2200	8.82×10^{-6}

2.6 Simulated concentrations and gas expansion factor

Because the 0D model operates at constant pressure, meaning constant total density, a correction factor is needed when comparing densities at different positions in the plasma, similar to the correction factor for gas expansion from section 1.2. In this instance, the total mass density ρ_{tot} is used to correct the density values in the model. For example, conversion is calculated as:

$$\chi_i^{sim} = \frac{n_i^{in} - \left(\frac{\rho_{tot}^{in}}{\rho_{tot}^{out}}\right) \cdot n_i^{out}}{n_i^{in}} = \frac{n_i^{in} - \alpha_{sim} \cdot n_i^{out}}{n_i^{in}} \qquad (S.E24)$$

For the confined APGD, not one but multiple simulations are used to describe the reactor (see section 2.5). The overall density of a species s should be determined first by means of equation (S.E25):

$$(\alpha_{sim} \cdot n_s) = \sum_{sim} fr_{sim} \cdot n_{s,sim} \cdot \left(\frac{\rho_{tot}^{in}}{\rho_{tot}^{out}}\right) \qquad (S.E25)$$

With fr_{sim} equal to the fraction of the reactor area that is represented by that simulation. Note that these density values are already corrected for gas expansion. However, to compare with the experimental results, the densities should be translated into concentrations. This is easily done by dividing each overall density by the total overall density $\sum_t(\alpha_{sim} \cdot n_t)$:

$$c'_s = \frac{(\alpha_{sim} \cdot n_s)}{\sum_t(\alpha_{sim} \cdot n_t)} \cdot 100\ \% \qquad (S.E26)$$

The change from density (in cm^{-3}) towards concentration (%) also implies an additional correction when comparing two values at different positions in the plasma, which is done by multiplying with an "overall" correction factor with exactly the same meaning as α' from section 1.2. This factor is equal to the ratio of the total overall outlet density over the total overall inlet density:

$$\alpha'_{sim} = \frac{\sum_t\left(\alpha_{sim}^{out} \cdot n_t^{out}\right)}{\sum_t\left(\alpha_{sim}^{in} \cdot n_t^{in}\right)} \qquad (S.E27)$$

Where $\alpha_{sim}^{in} = 1$ and $\sum_t n_t^{out} = \sum_t n_t^{in}$. With the overall concentration c'_s for any species s and gas expansion factor α'_{sim}, the experimental formulas in section 1.3 can be used directly without changes.

3 Additional experimental and calculation results

3.1 Selectivity and yield at other conditions than presented in the main paper

Varying CH_4 fraction at 35 mA and 1 L/min:

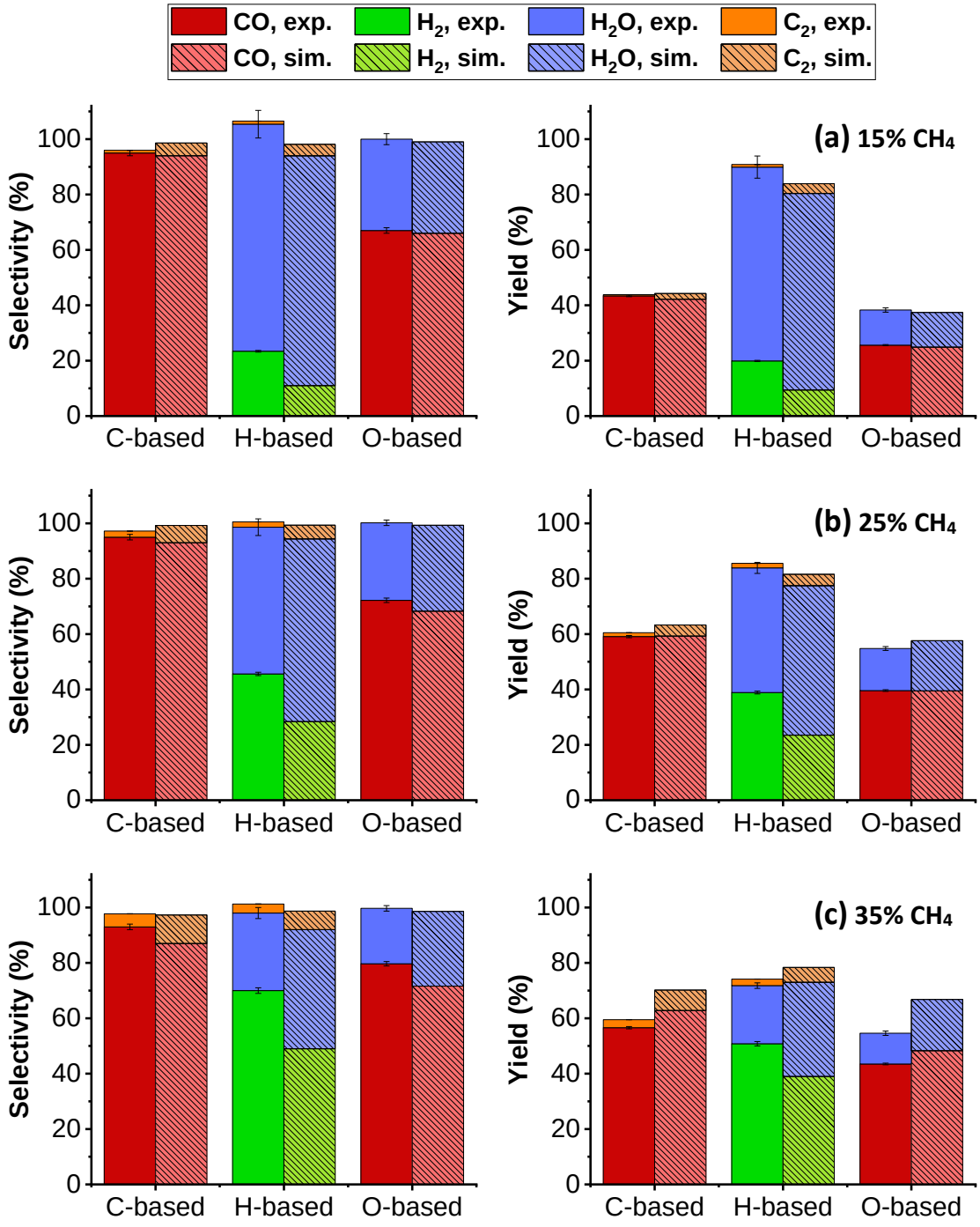

Figure S.9: Experimental and simulated C-, H- and O-based selectivities (left) and yields (right) for 15 (a), 25 (b) and 35% (c) CH_4 at 35 mA and 1 L/min. C_2H_2, C_2H_4 and C_2H_6 are grouped together as "C_2" but C_2H_2 is the major component (~ 72 (a), 82 (b) and 88% (c) of the total C_2-fraction). Error bars are added for the experimental results, but are often too small to be visible.

Varying current at 25% CH_4 and 1 L/min:

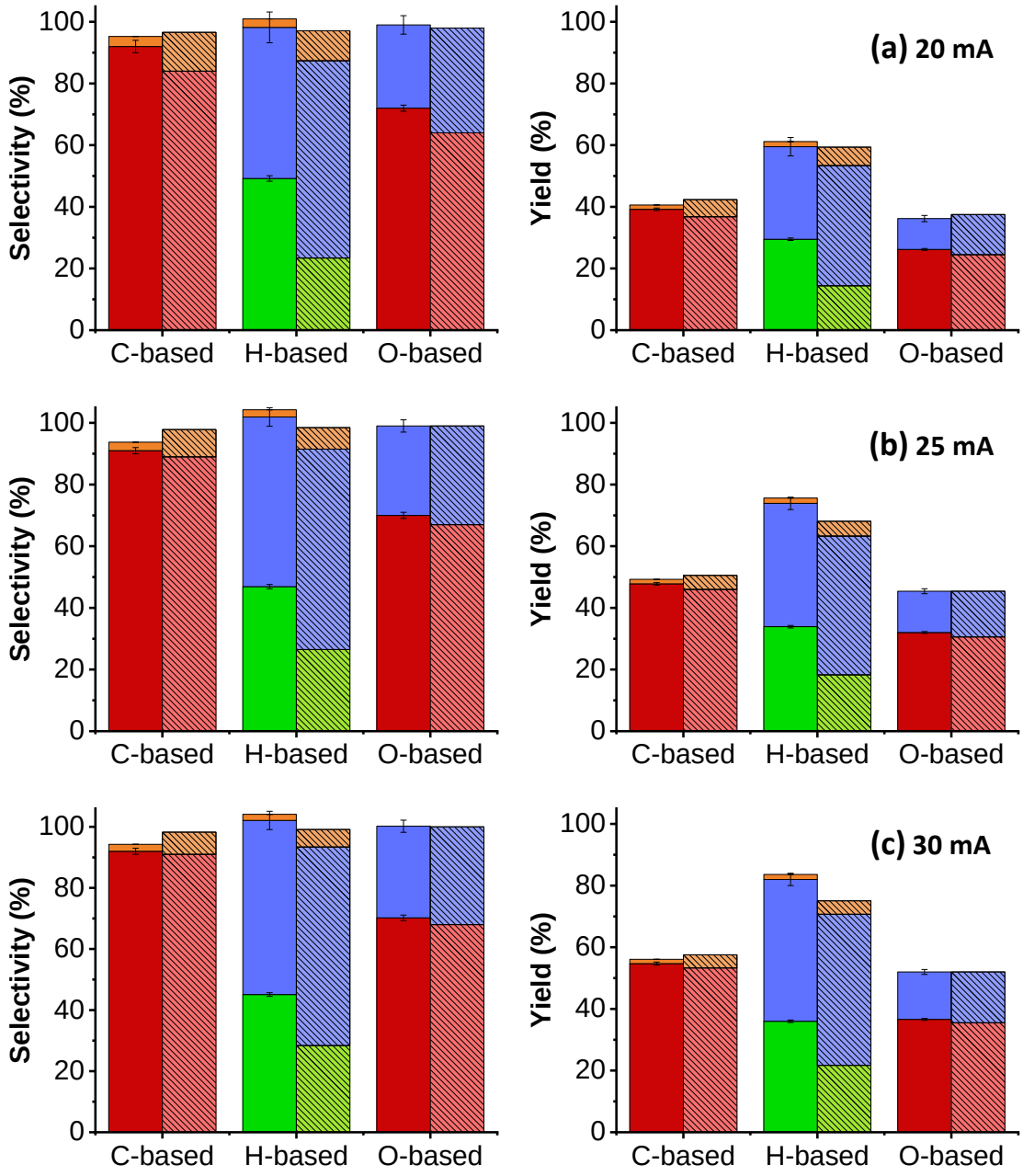

Figure S.10: Experimental and simulated C-, H- and O-based selectivities (left) and yields (right) for 20 (a), 25 (b) and 30 mA (c) at 25% CH_4 and 1 L/min. C_2H_2, C_2H_4 and C_2H_6 are grouped together as "C_2" but C_2H_2 is the major component (~ 84 (a), 83 (b) and 83% (c) of the total C_2-fraction). Error bars are added for the experimental results, but are often too small to be visible.

Varying flow rate at 25% CH_4 and 25 mA:

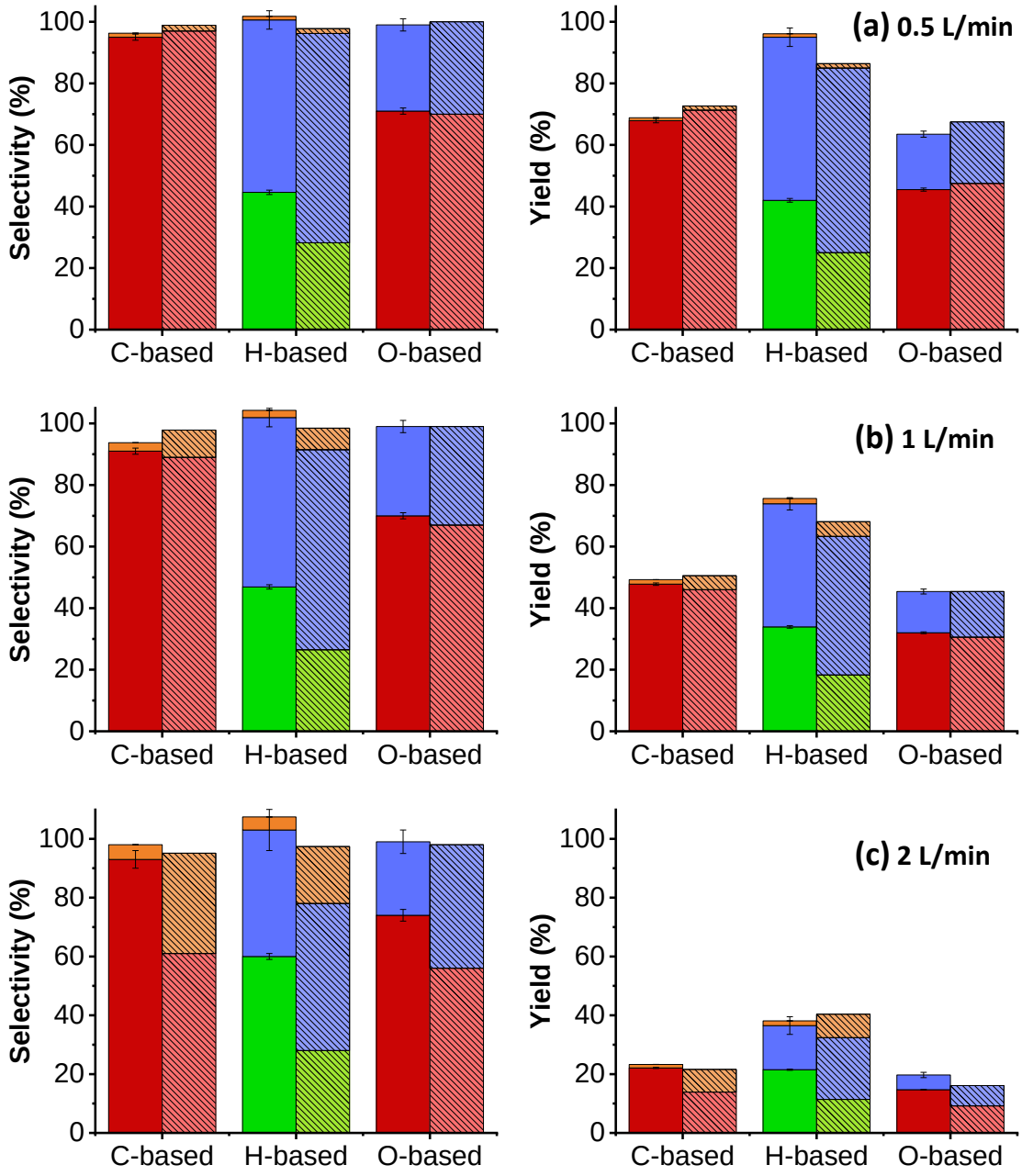

Figure S.11: Experimental and simulated C-, H- and O-based selectivities (left) and yields (right) for 0.5 (a), 1 (b) and 2 L/min (c) at 25% CH_4 and 25 mA. C_2H_2, C_2H_4 and C_2H_6 are grouped together as "C_2" but C_2H_2 is the major component (~ 79 (a), 83 (b) and 76% (c) of the total C_2-fraction). Error bars are added for the experimental results, but are often too small to be visible.

3.2 Vibrational distribution function of CO_2

The vibrational distribution function (VDF) of CO_2 exhibits no overpopulation of the highest vibrational levels, compared to a thermal or Boltzmann distribution. The VDF of CO_2 is plotted in Figure S.12 for 25% CH_4, 30 mA and 1 L/min, but for the other conditions exactly the same trend is observed.

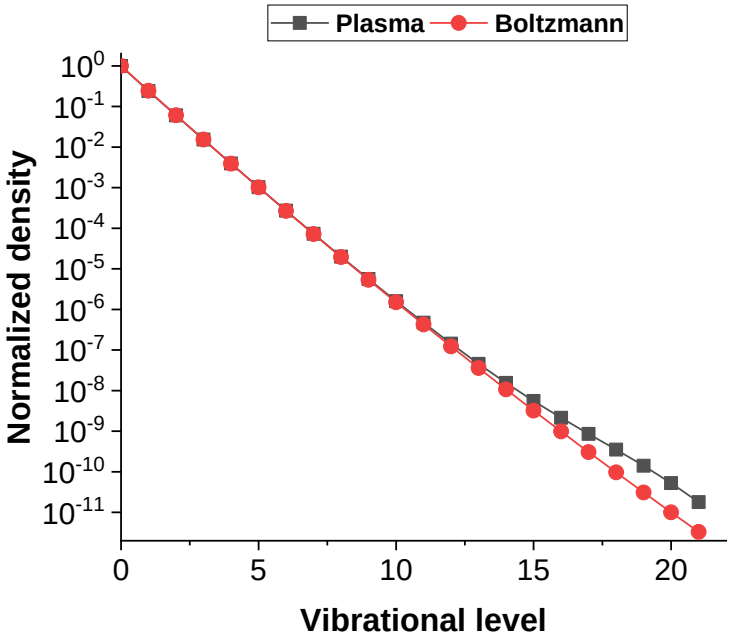

Figure S.12: Vibrational distribution function of CO_2 derived from the quasi-1D model, at 25% CH_4, 30 mA and 1 L/min.

References

(1) Pinhão, N.; Moura, A.; Branco, J. B.; Neves, J. Influence of Gas Expansion on Process Parameters in Non-Thermal Plasma Plug-Flow Reactors: A Study Applied to Dry Reforming of Methane. *Int. J. Hydrogen Energy* **2016**, *41* (22), 9245–9255. https://doi.org/10.1016/j.ijhydene.2016.04.148.

(2) Pancheshnyi, S.; Eismann, B.; Hagelaar, G. J. M.; Pitchford, L. C. Computer Code ZDPlasKin. http://www.zdplaskin.laplace.univ-tlse.fr/ (University of Toulouse, LAPLACE, CNRS-UPS-INP, Toulouse, France, 2008).

(3) Manion, J. A.; Huie, R. E.; Levin, R. D.; Jr., D. R. B.; Orkin, V. L.; Tsang, W.; McGivern, W. S.; Hudgens, J. W.; Knyazev, V. D.; Atkinson, D. B.; Chai, E.; Tereza, A. M.; Lin, C.-Y.; Allison, T. C.; Mallard, W. G.; Westley, F.; Herron, J. T.; Hampson, R. F.; Frizzell, D. H. NIST Chemical Kinetics Database, NIST Standard Reference Database 17, Version 7.0 (Web Version), Release 1.6.8, Data version 2015.09, National Institute of Standards and Technology, Gaithersburg, Maryland, 20899-8320. https://kinetics.nist.gov/ (accessed Jun 24, 2021).

(4) Hagelaar, G. J. M.; Pitchford, L. C. Solving the Boltzmann Equation to Obtain Electron Transport Coefficients and Rate Coefficients for Fluid Models. *Plasma Sources Sci. Technol.* **2005**, *14* (4), 722–733. https://doi.org/10.1088/0963-0252/14/4/011.

(5) Pitchford, L. C.; Alves, L. L.; Bartschat, K.; Biagi, S. F.; Bordage, M. C.; Bray, I.; Brion, C. E.; Brunger, M. J.; Campbell, L.; Chachereau, A.; Chaudhury, B.; Christophorou, L. G.; Carbone, E.; Dyatko, N. A.; Franck, C. M.; Fursa, D. V.; Gangwar, R. K.; Guerra, V.; Haefliger, P.; Hagelaar, G. J. M.; Hoesl, A.; Itikawa, Y.; Kochetov, I. V.; McEachran, R. P.; Morgan, W. L.; Napartovich, A. P.; Puech, V.; Rabie, M.; Sharma, L.; Srivastava, R.; Stauffer, A. D.; Tennyson, J.; de Urquijo, J.; van Dijk, J.; Viehland, L. A.; Zammit, M. C.; Zatsarinny, O.; Pancheshnyi, S. LXCat: An Open-Access, Web-Based Platform for Data Needed for Modeling Low Temperature Plasmas. *Plasma Processes and Polymers*. Wiley-VCH Verlag January 1, 2017, p 1600098. https://doi.org/10.1002/ppap.201600098.

(6) Kelly, S.; Bogaerts, A. Joule, in Press.

(7) Trenchev, G.; Nikiforov, A.; Wang, W.; Kolev, S.; Bogaerts, A. Atmospheric Pressure Glow Discharge for CO2 Conversion: Model-Based Exploration of the Optimum Reactor Configuration. *Chem. Eng. J.* **2019**, *362* (December 2018), 830–841. https://doi.org/10.1016/j.cej.2019.01.091.

(8) Cleiren, E.; Heijkers, S.; Ramakers, M.; Bogaerts, A. Cover Feature: Dry Reforming of Methane in a Gliding Arc Plasmatron: Towards a Better Understanding of the Plasma Chemistry (ChemSusChem 20/2017). *ChemSusChem* **2017**, *10* (20), 3864–3864. https://doi.org/10.1002/cssc.201701891.

(9) Kozàk, T.; Bogaerts, A. Splitting of CO2 by Vibrational Excitation in Non-Equilibrium Plasmas: A Reaction Kinetics Model. *Plasma Sources Sci. Technol.* **2014**, *23* (4), 045004. https://doi.org/10.1088/0963-0252/23/4/045004.

(10) Fridman, A. Plasma Chemistry. *Plasma Chem.* **2008**, *9780521847353*, 1–978. https://doi.org/10.1017/CBO9780511546075.

(11) Wang, W.; Snoeckx, R.; Zhang, X.; Cha, M. S.; Bogaerts, A. Modeling Plasma-Based CO2 and CH4 Conversion in Mixtures with N2, O2, and H2O: The Bigger Plasma Chemistry Picture. *J. Phys. Chem. C* **2018**, *122* (16), 8704–8723. https://doi.org/10.1021/ACS.JPCC.7B10619/SUPPL_FILE/JP7B10619_SI_001.PDF.